Title

Microstructural changes to the brain of mice after methamphetamine exposure as identified with diffusion tensor imaging

Authors

McKenna, Benjamin S

Brown, Gregory G

Archibald, Sarah

et al.

Publication Date

2016-03-01

DOI

10.1016/j.pscychresns.2016.02.009

Peer reviewed

HHS Public Access

Author manuscript

Psychiatry Res. Author manuscript; available in PMC 2017 March 30.

Published in final edited form as:

Psychiatry Res. 2016 March 30; 249: 27–37. doi:10.1016/j.pscychresns.2016.02.009.

Microstructural Changes to the Brain of Mice after Methamphetamine Exposure as Identified with Diffusion Tensor Imaging

Benjamin S. McKenna[a,1], **Gregory G. Brown**[a,*], **Sarah Archibald**[a], **Miriam Scadeng**[b], **Robert Bussell**[b], **James P. Kesby**[a], **Athina Markou**[a], **Virawudh Soontornniyomkij**[a], **Cristian Achim**[a], and **Svetlana Semenova**[a]

[a]Department of Psychiatry, School of Medicine, University of California, San Diego, 9500 Gilman Drive, M/C 0603, La Jolla, CA 92093, USA

[b]Department of Radiology, School of Medicine, University of California, San Diego, 200 West Arbor Drive, M/C 0834, La Jolla, CA 92103, USA

Abstract

Methamphetamine (METH) is an addictive psychostimulant inducing neurotoxicity. Human magnetic resonance imaging and diffusion tensor imaging (DTI) of METH-dependent participants find various structural abnormities. Animal studies demonstrate immunohistochemical changes in multiple cellular pathways after METH exposure. Here, we characterized the long-term effects of METH on brain microstructure in mice exposed to an escalating METH binge regimen using *in vivo* DTI, a methodology directly translatable across species. Results revealed four patterns of differential fractional anisotropy (FA) and mean diffusivity (MD) response when comparing METH-exposed (n=14) to saline-treated mice (n=13). Compared to the saline group, METH-exposed mice demonstrated: 1) decreased FA with no change in MD [corpus callosum (posterior forceps), internal capsule (left), thalamus (medial aspects), midbrain], 2) increased MD with no change in FA [posterior isocortical regions, caudate-putamen, hypothalamus, cerebral peduncle, internal capsule (right)], 3) increased FA with decreased MD [frontal isocortex, corpus callosum (genu)], and 4) increased FA with no change or increased MD [hippocampi, amygdala, lateral thalamus]. MD was negatively associated with calbindin-1 in hippocampi and positively with dopamine transporter in caudate-putamen. These findings highlight distributed and differential

*Corresponding Author:Gregory G. Brown La Jolla Corporate Center Suite 224/226 3252 Holiday Ct. La Jolla CA, 92037. gbrown@ucsd.edu.

[1]The Translational Methamphetamine AIDS Research Center (TMARC) Group

Authors Contributions

GG, SA, MS, RB, AM, JK, CA, and SS were responsible for the study concept and design. JK, AM, and SS contributed to the methamphetamine and saline regimens and care of animals. SA, MS, and RB contributed to the neuroimaging acquisition and transfer of animal data. BM and GG processed, analyzed, and interpreted the neuroimaging data. CA and VS processed and analyzed the immunohistochemical data. BM drafted the manuscript and all authors critically reviewed the content and approved the final version for publication.

METH effects within the brain suggesting several distinct mechanisms. Such mechanisms likely change brain tissue differentially dependent upon neural location.

Keywords

diffusion tensor imaging; fractional anisotropy; magnetic resonance imaging; mean diffusivity; methamphetamine; mouse

1. Introduction

Methamphetamine (METH) is an addictive psychostimulant that induces central nervous system toxicity and associated neurocognitive impairment, such as impaired behavioral inhibition and attentional control (Nordahl et al., 2003; Scott et al., 2007). Cognitive deficits are thought to be due to a wide variety of neurotoxic effects from METH exposure that induce long lasting changes to the structure and function of the brain (Büttner, 2011). In humans, much of what is known about the impact of METH on the brain comes from magnetic resonance imaging (MRI) studies of adult METH users. These cross-sectional studies have demonstrated structural abnormalities in the frontal lobe, including lower gray matter density or volumes (Kim et al., 2006; Schwartz et al., 2010), larger white matter volumes (Bartzokis et al., 2001), and increased white matter hyperintensities (Berman et al., 2008). Moreover, smaller volumes have been observed in the temporal lobe (Bartzokis et al., 2000), including the hippocampus (Thompson et al., 2004); whereas larger volumes have been observed in the parietal cortex (Jernigan et al., 2005) and striatal regions (Chang et al., 2005) of adult METH users.

It has been speculated that enlarged brain regions reflect inflammatory changes whereas reductions in size reflect neuronal cell loss (Thompson et al., 2004), but the mechanisms remain unclear. Recently, diffusion tensor imaging (DTI) has been used to examine microstructural brain changes associated with METH. By linking macroscopic brain changes to microscopic cellular events, DTI promises to integrate large scale brain changes to cellular changes, providing a more integrated view of the effects of a pathological agent on neural systems than does conventional MRI (Bammer et al., 2006). DTI provides quantitative information about the geometric distribution of water diffusion within imaging voxels (Basser, 2006). An aim of DTI is to infer information about the integrity of tissue microstructure from this geometric information. Inferences from diffusion data are typically based on the biological boundary model, which states that at sufficiently long diffusion times, water molecules in biological tissues will diffuse in an isotropic manner until they reach a membrane or large protein boundary (Chanraud et al., 2010; Le Bihan and Johansen-Berg, 2012). Such cell boundaries are believed to reduce overall diffusion magnitude and shape the direction of water movement. Based on this geometric information several measures can be computed including mean diffusivity (MD) and fractional anisotropy (FA), the later a measure of the degree to which water movement is dominated by a single direction (Basser, 2006). Based on the biological boundary model, reduced FA and increased MD implies reduced density of membranes possibly due to tissue loss (Alicata et al., 2009). DTI changes associated with METH abuse or dependence have commonly revealed lower

FA in frontal white matter and increased MD in basal ganglia structures, such as the putamen and caudate (Alicata et al., 2009; Chung et al., 2007; Tobias et al., 2010). Differences in the integrity of the corpus callosum are less often found, with some investigators reporting lower FA values in the genu (Kim et al., 2009; Tobias et al., 2010), whereas others report only trends or no callosal effect (Alicata et al., 2009; Salo et al., 2009). When cognition is investigated, lower FA in regions within the frontal cortex or genu has been associated with worse cognitive performance (Chung et al., 2007; Salo et al., 2009).

However, human MRI and DTI studies of METH use have several acknowledged limitations. DTI studies only examined only a few regions of interest within the brain, and all studies used cross-sectional designs that do not disentangle markers that predate drug use, effects of abstinence duration, and different use patterns. Further, differences in the maximal dose, days of usage per week/month, and total quantity of METH intake along with polysubstance abuse among participants could result in different neuropathological and cognitive outcomes (Berman et al., 2008; Salo and Fassbender, 2012). Given the challenges of establishing the direct effects of METH in humans, investigators have performed animal experiments to obtain basic neuroscience data on METH exposure. In mice, exposure to neurotoxic METH doses led to decreased dopamine function in the cortex and striatum. For example, decreases in dopamine (Achat-Mendes et al., 2005; Fantegrossi et al., 2008) and tyrosine hydroxylase levels (Achat-Mendes et al., 2005; Bowyer et al., 2008; Deng et al., 1999; Fantegrossi et al., 2008) in the striatum and cortex suggest decreased dopaminergic innervation after METH exposure. METH also induces neuronal death in the striatum, frontal and parietal cortices, hippocampus, and olfactory bulb in a process akin to neuronal apoptosis (Cadet et al., 2005; Cunha-Oliveira et al., 2008); as well as leading to reactive astrocytosis (Deng et al., 1999; Zhu et al., 2005) and microgliosis (Bowyer et al., 2008; Fantegrossi et al., 2008; Thomas and Kuhn, 2005). Within the caudate-putamen METH-induced dopaminergic neurotoxicity has been found to be mediated by the dopamine transporter [DAT; (Fumagalli et al., 1998)]. Given the evidence that METH has a variety of effects on neuronal structure and function at the cellular level in animals and at the brain systems level in humans, it is unfortunate that there has been little work using neuroimaging to directly link these two levels of neural organization. New knowledge from tightly controlled animal experiments employing the same *in vivo* neuroimaging techniques as those used in human studies offers a powerful translational context to better understand the impact of METH on the brain.

The aim of the present study was to utilize DTI in mice previously exposed to a METH binge regimen in order to characterize the long-term effects of METH on the microstructure of the brain using neuroimaging techniques that are translatable across species. Consistent with evidence for METH-induced tissue damage, we hypothesize that decreased FA will be associated with increased MD in METH-exposed mice compared to saline control mice within the frontal and striatal gray matter and their connecting pathways, hippocampus, and white matter tracts such as the corpus callosum and internal capsule. In addition, the whole brain was examined to explore additional microstructural DTI changes given the heterogeneity of METH effects including the potentially differential impact on neuronal cell bodies and their processes versus surrounding glial and astrocyte cells. In exploratory

analyses we also investigated potential associations between DTI markers of tissue damage and cellular changes in the caudate-putamen and hippocampus, two brain regions known to be adversely impacted by METH. Specifically, we examined links between MD and immunohistochemical assays of DAT in the caudate-putamen and calibindin-1 in the dorsal hippocampi of a subgroup of METH-exposed mice. Calibindin-1, a marker of hippocampal function associated with calcium buffering, has been implicated in the effects of METH (Kuczenski et al., 2007).

2. Methods

2.1. Animals

This study was part of a larger examination of the individual and combined effects of human immunodeficiency virus and METH conducted by The Translational Methamphetamine AIDS Research Center (TMARC). Male mice from a C57BL/6×DBA (BDF1) genetic background (N=27) were tested in the current study. Mice were grouped-housed with 2–4 mice per group in a climate-controlled environment with a reversed day/night cycle (lights on at 19:00 h, off at 07:00 h). Since mice are nocturnal animals and active during night, the day/night cycle was reversed so that behavioral assessments could occurred during the day. For MRI mice were housed under the same conditions for consistency. The animals were given free access to food (diet #8626, Haran Teklad, Madison, Wisconsin, USA) and water for the duration of the testing. All procedures were approved by the UCSD Institutional Animal Care and Use Committee and conformed to NIH guidelines. Mice were 4–5 months old at the beginning of study procedures and 9–10 months old at time of MRI, (see below). These mice were previously tested in a battery of cognitive tasks (Kesby et al., 2015a; Kesby et al., 2015b).

2.2. Methamphetamine regimen

METH (Sigma, St. Louis, Missouri, USA) was dissolved in saline and administered subcutaneously with a 5ml/kg injection volume (doses are expressed as salt). Stock solutions of the drug were prepared every three to four days and diluted as needed during the drug regimen. Mice were exposed to an escalating dose-multiple binge METH regimen that was originally established in rats (Kuczenski et al., 2007). While the neurotoxic effects of METH have been typically induced by an acute “binge” procedure (4 injections of high doses in drug-naïve rodents; Davidson et al., 2001), it has been postulated that the inclusion of an escalating dose pretreatment regimen represents a more accurate simulation of the gradual dose progression in human abusers (Segal and Kuczenski, 1997). Prior work indicated that inclusion of this escalation paradigm attenuates the hyperthermic effects of higher METH doses in rats, while still inducing neuropathological and behavioral effects in both rats and mice (Henry et al., 2013; Kesby et al., 2015a; Kesby et al., 2015b; Kuczenski et al., 2007). Mice were treated three times per day (10:00; 13:15; 17:30 h) for 14 days with vehicle (saline; n=13) or escalating doses of METH (n=14), starting with 0.1mg/kg and increasing to 4.0mg/kg, with a stepwise increase of 0.1mg/kg per injection. After this 14-day period, animals received four daily injections of 6.0mg/kg METH or vehicle at 2-h intervals (10:00, 12:00, 14:00, and 16:00 h) during an 11-day ‘binge’ period (Figure 1).

2.3. Imaging acquisition

In vivo MRI scanning was conducted 3–4 months post-METH between 09:00 and 18:00 when mice were 9–10 months old. Experiments were conducted at the UCSD Center for Functional MRI using a Bruker 7.0T/20cm horizontal magnet with Avance II hardware (Bruker, Billerica, MA, USA). Mice were anesthetized with an isoflurane-oxygen mixture (2.0 vol% with an oxygen flow of 1.2–1.4 l/min) in order to minimize motion throughout the session. Mice were positioned prone in an animal holder with foam pads on each side of the head, front teeth were hooked onto a bite bar, and the shoulders secured with tape to further minimize head movement. Body temperature was monitored by a rectal thermometer and kept at ~37° C core temperature using warm airflow. At the beginning of each imaging session, a high resolution anatomical dataset was collected using a RARE (Rapid Acquisition with Relaxation Enhancement) pulse sequence in order to facilitate anatomical localization and to define regions of interest (TR/TE=9247/35ms, RARE factor=8, bandwidth=35714Hz, field of view 21.0mm-x-16.1mm, matrix 140-x-107, inplane resolution 150μm-x-150μm, 80 slices 150μm thick, averages=16, flip angle 85°, time=24min). A navigated, 30 direction, 4-shot, spin echo DTI-EPI protocol with b=1000s/mm^2, 5 b=0s/mm^2 images, partial k-space and zero filling in the read direction. The flip angle was 90°, TR/TE 7500/23.34ms, bandwidth=250kHz, FOV 26.4mm-x-12.0mm, reconstructed matrix 176-x-80, inplane resolution 150μm-x-150μm, 30 slices 600μm thick, 1 average, time=17.5min. To correct for signal bias, minimum contrast images was acquired after both T2 and DTI scans. Minimum contrast scans were collected with TR/TE=9000/7.3ms, RARE factor=4, bandwidth=8333Hz, field of view 21.0mm-x-16.1mm, matrix 140-x-107, inplane resolution 150μm-x-50μm, 80 slices 160μm thick, averages=16, flip angle 90°, time=3min. Data were acquired using a two channel local receive coil combined with a 72 mm ID birdcage volume transmitter.

2.4. Image processing

Analysis of Functional NeuroImaging [AFNI; (Cox, 1996)] and UCSD developed software was used to process images. Diffusion tensors were calculated at the end of the imaging session using software available in Paravision after correcting for eddy currents. This step produces S_0 [The echo image intensity with no applied graduates (Basser et al., 1994)], FA, trace, and three eigenvalue and three eigenvector maps. FA was calculated using standard formulas (Basser, 2006). The eigenvalue maps were used to calculate MD (the average of the 3 eigenvalues λ1, λ2, and λ3) as well as axial diffusivity (λ1) and radial diffusivity (average of λ2 and λ3). T2 images were intensity bias corrected using the minimum contrast images to correct for field inhomogeneity. Skull and extraneous tissue were removed from the images using the AFNI 3dSkullStrip tool with the rat option selected and, when needed, manual editing in AFNI. For group analyses, images were warped into the Waxholm Space (WHS) Atlas (Johnson et al., 2010) of the C57BL/6 mouse brain using a 12 parameter affine transformation. The intensity-bias corrected, skull stripped T2 data were warped into WHS atlas resulting in an average Dice index of 0.987, indicating nearly perfect overlay between registered the T2 volumes and the WHS atlas (Dice, 1945). DTI images were then transformed into WHS by realigning the DTI images with the WHS transformed T2 image from the same session. Specifically, for the DTI images the bias-corrected skull-stripped S_0

image was realigned to the WHS T2 with the resulting transformation matrix applied to the DTI maps.

2.5. Immunohistochemistry and quantitative image analysis

After *in vivo* MRI scanning was completed, a subgroup of METH-exposed mice were humanely euthanized and brain samples were collected for immunohistochemical analyses. Immunoperoxidase staining was performed on nine of the METH-exposed mice. Staining was done on 5μm-thick paraffin-embedded paraformaldehyde-fixed coronal brain sections with anti-calbindin-1 antibody (#AB1778, Millipore, Billerica, MA, USA, 1:300 dilution) and anti-DAT (6-5G10, #sc-3258, Santa Cruz Biotechnology, Santa Cruz, CA, USA, 1:100), as described previously (Soontornniyomkij et al., 2010). The immunostained slides were digitally scanned (Aperio ScanScope GL, Vista, CA, USA). The immunoreactivity intensity was measured within (Image-Pro Analyzer software, Version 6.3, Media Cybernetics, Bethesda, MD, USA) and normalized to the anatomic area, i.e., the combined hippocampal CA1 strata oriens, pyramidale, radiatum, and lacunosum-moleculare for calbindin-1; and the caudate-putamen for DAT, as previously described (Soontornniyomkij et al., 2010).

2.6. Statistical analyses

DTI parameters FA and MD were compared separately between the METH-exposed and saline control groups using independent-samples t-tests for voxels within the whole brain. A two-step procedure was used to adjust for multiple statistical tests in order to control for the expected proportion of clusters incorrectly rejected under the null hypothesis that DTI values did not differ between groups. First, we identified clusters of voxels with voxel-wise significance $p<0.05$ and then corrected for multiple comparisons. To correct for multiple comparisons we calculated the proportion of clusters of a given size from all voxels analyzed within the whole brain under the null hypothesis for a nearest neighbor connectivity rule, voxel-wise p-value of 0.05, and a Gaussian filter width (FWHM) of 220μm. The FWHM was chosen based on the average FWHMs across each in-plane axis averaged across all mice taking into account the underlying structure in the FA and MD volumes. Based on these calculations we defined significant clusters at a threshold of 0.081μL corresponding to a corrected p-value of 0.05 for multiple comparisons. This further corresponds to the expected number of falsely detected clusters under the null hypothesis of no group difference. Mean values for each analysis type (i.e., FA and MD) were extracted from each significant cluster, in addition to radial and axial diffusivity values, to calculate effect sizes and better interpret the diffusivity patterns between groups. Anatomical locations for each significant cluster were localized using the WHS atlas (Johnson et al., 2010), Paxinos and Hamilton atlas (Paxinos and Franklin, 2001), and Allen mouse brain atlas, available online at http://www.brainmap.org/. Cohen's d effect size parametric maps were also calculated across the whole brain from the T-tests for FA and MD.

For immunohistochemistry analyses the association between MD and calbindin-1 immunoreactivity intensity was examined within the dorsal hippocampi defined by the WHS Atlas labels using linear regression. Similarly, the association between MD and DAT immunoreactivity intensity was examined within the caudate-putamen. Because interpreting abnormal MD as a marker of tissue damage is less controversial in gray matter than are

interpretations based on FA, only analyses involving MD are reported (Beaulieu, 2002). Given the limited sample sizes used for immunohistochemistry analyses, it is unlikely that statistically significant differences in correlation between the METH exposed and saline-exposed groups would be detected. Therefore only correlations for the METH group are reported. Specifically, effect size maps (R^2) were created with the direction of the association preserved to examine the relationship between MD and immunohistochemical markers within the METH group. A per-voxel threshold of ±0.25 R^2 was applied to limit interpretation to large effect sizes accounting for at least 25% of the variance (Cohen, 1988). A threshold of 0.081μL was applied to effect size clusters within the region of interest to examine spatially continuous clusters of effect similar to our main analyses.

3. Results

3.1. Fractional anisotropy

Individual mouse FA maps were checked to examine registration to the WHS atlas. The highest FA values, in the range of 0.5–0.7, were constrained to voxels within the WHS corpus callosum, optic chiasm, external capsule, and internal capsule demonstrating good correspondence to WHS atlas space. This was also true for voxels entirely within these white matter tracts in native space (i.e., range of 0.5–0.8). Figure 2a illustrates Cohen's d effect size parametric maps for differences in FA between METH and saline groups within the whole brain highlighting both increased and decreased FA within different regions. Table 1 presents clusters where there was a significant difference in FA with a corrected p-value <0.05; as well as axial and radial diffusivity values to facilitate interpretation of FA changes, and effect sizes for all variables. There was significantly increased FA in several regions within the frontal isocortex, hippocampus, amygdala, lateral thalamus, and genu of the corpus callosum extending into the motor area in the METH group. By contrast, decreased FA was observed in other posterior regions within the midbrain, medial thalamus, posterior forceps of the corpus callosum extending into the subiculum, and internal capsule extending into the caudate-putamen (Figure 2c and Table 1). As FA is a standardized metric of the degree to which water movement is not equidimensional, increases or decreases to FA may be due to different patterns of change to the underlying geometry of the ellipsoids. Figure 3a presents two examples of increased FA from our results comparing the isocortex to the hippocampi (see discussion) and one example of decreased FA. Increased FA in the METH group compared to the saline group within the isocortex was due to greater reductions in radial versus axial diffusivity; whereas in the increased FA in bilateral hippocampi were due to increased axial diffusivity. In the example of the corpus callosum extending into the subiculum, decreased FA resulted from reduced axial and increased radial diffusivity. To aid in the interpretation of the significant FA effects, values for radial and axial diffusivity are presented in Table 1.

3.2. Mean diffusivity

Figure 2b illustrates non-threshold Cohen's d effect size parametric maps for a separate analysis examining differences in MD between METH and saline groups within the whole brain. Table 2 presents clusters where there was a significant difference in MD with a corrected p-value <0.05; as well as axial and radial diffusivity values to facilitate

interpretation of FA changes, and effect sizes for all variables. There was significantly increased MD in several posterior regions in the isocortex and in hippocampi, hypothalamus, caudate-putamen, cerebral peduncle and internal capsule extending into the amygdala, and genu of the corpus callosum extending into the anterior cingulate in the METH group. Alternatively, decreased MD was observed only in two regions overlapping with clusters of increased FA in the frontal isocortex (Figure 2c and Table 2). Figure 3b presents an example of increased MD in METH-exposed mice compared to saline control mice within the caudate-putamen. In this case axial and radial diffusivity increased by similar amounts. Table 2 presents axial and radial diffusivity findings along with the MD effects.

3.3 Immunohistochemistry

Figure 4 presents the associations between MD and calbindin-1 and DAT immunoreactivity intensities with the METH-exposed group. Given the limited sample size of the immunohistochemical assays we focused our analyses on effect sizes within the METH-exposed sample. Large effects were observed such that increased MD was associated with decreased calbindin-1 in the dorsal hippocampi among mice exposed to METH. Large effects were also observed in the caudate-putamen such that increased MD was associated with increased DAT among mice exposed to METH.

4. Discussion

Using *in vivo* DTI we demonstrated long lasting spatially distinct patterns of change in the brain tissue of mice previously exposed to a one-month METH binge regimen compared to saline controls. Contrary to the hypothesis that METH-induced tissue damage would lead to decreased FA coupled with increased MD, we found that METH exposure induced significantly increased FA in the frontal areas of the isocortex including the motor and somatosensory areas, as well as the genu of the corpus callosum. Increased FA was also observed in medial temporal lobe structures, such as the hippocampus and amygdala, as well as lateral aspects of the thalamus. In contrast to these findings, decreased FA was observed in posterior forceps of the corpus callosum, internal capsule, subiculum, caudate-putamen, medial aspects of the thalamus, and midbrain gray matter consistent with METH-induced tissue damage. When examining MD, we found many areas demonstrating significantly increased diffusivity in more posterior cortical areas including visual, auditory, perirhinal, and ectorhinal areas and the caudate-putamen, dorsal and ventral hippocampi, amygdala, hypothalamus, amygdala, cerebral peduncle, internal capsule, and the genu of the corpus callosum. Areas of significantly decreased MD overlapped with significant clusters of increased FA in the motor and somatosensory areas.

Overall, four distinct patterns of FA and MD change between METH-exposed versus saline-treated control mice were observed: 1) decreased FA with no change in MD, 2) increased MD with no change in FA, 3) increased FA with decreased MD, and 4) increased FA with no change or increased MD. The decreased FA and increased MD findings are consistent with and extend what has been observed in human studies that demonstrate METH-induced tissue damage, though analyses have been limited to select regions. For example, in humans decreased FA has been reported in the corpus callosum (Tobias et al., 2010) and increased

MD in the caudate (Alicata et al., 2009). Here, we observed the same pattern in similar regions in mice. However, we also observed decreased FA and/or increased MD in many other cortical grey matter regions not currently investigated in human DTI studies. These regions have been found to be vulnerable to METH exposure from human volumetric MRI studies and mouse immunohistochemical studies including the hippocampi (Cadet et al., 2005; Cunha-Oliveira et al., 2008; Thompson et al., 2004) and posterior cortical regions (Jernigan et al., 2005). Interestingly, we found evidence for increased FA and decreased MD in overlapping frontal cortical regions and mixed findings of increased FA and MD in distinct regions of the hippocampi. It is important to note that inferences on neural microstructure from DTI rely on acquired geometric information and changes to FA can be due to a variety of changes on the underlying geometry. For example, when examining radial and axial diffusivity measures in regions of increased FA in frontal isocortex versus hippocampi two different interpretative patterns emerged. In frontal regions increased FA was due to a reduction in both axial and radial diffusivity, but a greater reduction in radial diffusivity. Alternatively, increased FA in the hippocampi was primarily due to increased axial diffusivity (see Figure 3a). Thus, increases to FA may be due to different mechanisms in how METH affects cell structure in imaging voxels such as apoptosis versus astrocytosis. However, there is little data in METH-exposed animals or METH-dependent humans directly linking DTI findings to immunohistochemical characterization of cellular changes associated with METH exposure.

Our immunohistochemical findings suggest two possible mechanisms for METH-induced changes to MD in the caudate-putamen and dorsal hippocampus. Within the hippocampus, we found that decreased calbindin-1 was associated with increased MD in METH-exposed mice. It is possible that METH damages neuronal homeostasis through interrupting intracellular calcium signaling leading to tissue damage and, thereby increased diffusion of water as measured by DTI. Loss of calbindin interneurons in the hippocampus and/or the frontal cortex has been reported after exposure to a neurotoxic METH regimen in rats (Kuczenski et al., 2007) and was associated with cognitive deficits in METH users with HIV (Chana et al., 2006) and aged mice (Soontornniyomkij et al., 2012). Previously, we reported that spatial learning was impaired in METH-exposed mice including a subgroup of mice used in this study (Kesby et al., 2015b). Specifically, we found that methamphetamine exposure impaired spatial strategy during the Barnes maze test acquisition trials, indicating METH-induced hippocampal dysfunction. In this study, we found large METH effects in MD and FA within the hippocampus of a subset of these mice suggesting that DTI can be used to identify the neural substrate of behavioral deficits induced by METH, such as spatial learning. Given that hippocampal DTI changes were also associated with intensity of calbindin-1 expression, *in vivo* DTI may be an informative way to translate cellular to behavioral changes through examination of brain microstructure at the neural systems level of analysis.

Within the caudate-putamen, increased DAT was associated with increased MD in METH-exposed mice. Considering that the dopaminergic neurotoxicity effects of METH in dopamine pathways in the caudate-putamen are mediated by DAT (Fumagalli et al., 1998), it may be that increased tissue damage, as measured with MD, in METH-exposed mice is induced by increased DAT levels. However, loss of DAT during METH exposure with

significant recovery following protracted abstinence has been documented (Volkow et al., 2015). Given that our cross-sectional DTI scan and immunohistochemical analyses were 3–4 months after METH exposure it is unclear what the change in DAT levels were in our sample. Further research is needed to link the heterogeneous neural impact of METH found in DTI analyses with immunohistochemical and behavioral assays.

The biological boundary model suggests several additional testable biophysical hypotheses to explain the observed FA/MD patterns. For example, increased MD would be indicative of impaired membrane integrity such as demyelination or loss of cellular processes leading to increased diffusion. When interpreting human DTI data, investigators have speculated that increased “glial cellularity” or cell volume might lead to increased anisotropy and lower diffusivity due to increased extra-neuronal volume caused by glial activation in response to neuroinflammation (Alicata et al., 2009). Further, axonal growth or increased density of cellular processes in response to acute METH effects may lead to increased FA and/or decreased MD. Lastly, METH may cause increased intercellular swelling from cytotoxic edema leading to reduced radial diffusivity and thus increased FA and decreased MD. Animal studies provided some support for the membrane boundary model in explaining the potential impact of METH on the brain. Specifically, a limited yet instructive literature is available for cocaine-exposed rodents. Cocaine-exposed rats show lower FA in the genu and splenium of the corpus callosum and in the internal capsule (Narayana et al., 2009; Narayana et al., 2014). Myelin basic protein was reduced in the splenium of the corpus callosum and both myelin basic protein and neurofilament-heavy protein was reduced in the internal capsule (Narayana et al., 2014). The joint observation of lower FA and myelin basic protein supports the inference from the membrane boundary model that lower FA in white matter is associated with myelin loss. Evidence of increased expression of growth associated protein-43 in rats exposed to cocaine suggests that compensatory growth of axons and terminals, perhaps increasing density of neural processes, is possible and might alter FA values (Clarke et al., 1996; Narayana et al., 2014). In a rat traumatic brain injury model, increased FA in gray matter was associated with a very large increase in glial fibrillary acidic protein, with a smaller reduction in microtubule associated protein 2, supporting a prominent contribution of gliosis to increased FA (Budde et al., 2011). The authors speculated that the capacity of gray matter astrocytes to elongate as they activate might have caused the increase in FA.

There were some study features that limited interpretation of the data. DTI is limited to measuring both extracellular and intracellular water diffusion (Basser, 2006). As such, studies linking immunohistochemical markers with DTI will be vital in understanding what underlying mechanisms lead to changes in diffusivity patterns, which can then be translated to human MRI and behavioral studies. Within a subset of our METH-exposed sample we examined two immunohistochemical markers (DAT and calbindin-1) providing preliminary evidence for mechanisms that may cause DTI changes in the caudate-putamen and hippocampi. However, additional histology in multiple neuronal regions is needed to fully understand our DTI findings. While our analytic approach allowed us to examine clusters of differences between METH and saline control groups within the whole brain, several clusters involving the white matter also included surrounding gray matter. This is due, in part, to our voxel resolution as well as the anatomical structure of white matter in the mouse

brain leading to partial volume effects. Further, MRI was conducted 3–4 months following the binge regimen and thus did not capture the early effects of METH withdrawal. However, our work highlights the long-lasting effects of exposure to a METH binge regimen on the brain with medium to large effect sizes observed.

A strength of animal research is the ability to conduct tightly controlled experiments. Human METH studies inherently suffer from variability in drug use variables and heterogeneous samples. The present studies examined mice with identical genetic backgrounds treated similarly with the exception of METH versus saline dosing providing increased specificity of the METH effects on the brain compared to human studies. The present findings highlight distributed and differential METH effects within white and grey matter. This is not surprising given the diverse findings from basic neuroscience experiments suggesting that METH affects the brain through multiple pathways. As such, multifaceted immunohistochemical studies linking staining markers to DTI changes in METH-exposed mice are needed to clarify the cellular mechanisms underlying DTI findings. These future studies are likely to elucidate the etiology of MRI signal changes that can be then translated to human clinical samples. Our findings suggest that examination of microstructural changes in cortical regions with DTI could prove fruitful in human studies. Finally, our results support the use of DTI as an important translational tool able to be used with humans and animals.

Acknowledgments

Support for this study was provided by a National Institute on Drug Abuse (NIDA) Center award to the Translational Methamphetamine AIDS Research Center (TMARC, P50 DA26306), the Training in Research on Addictions in Interdisciplinary NeuroAIDS NIDA Grant (TRAIN, T32 DA031098 to BM), and the Interdisciplinary Research Fellowship in NeuroAIDS (IRFN, MH81482 to JK). TMARC is affiliated with the University of California, San Diego (UCSD), the Sanford-Burnham Medical Research Institute (SBMRI), and the University of California, Irvine (UCI). The TMARC is comprised of: Director – Igor Grant, M.D.; Co-Directors – Ronald J. Ellis, M.D., Ph.D., Scott L. Letendre, M.D., and Cristian L. Achim, M.D., Ph.D.; Center Manager – Mariana Cherner, Ph.D.; Associate Center Manager – Erin E. Morgan, Ph.D.; Assistant Center Manager – Aaron M. Carr, B.A.; Behavioral Assessment and Medical (BAM) Core – Neuromedical and Laboratory Unit (NLU): Scott L. Letendre, M.D. (Core Co-Director/NLU Chief), Ronald J. Ellis, M.D., Ph.D.; BAM Core–Neuropsychiatric Unit (NPU): Robert K. Heaton, Ph.D. (Core Co-Director/NPU Chief), J. Hampton Atkinson, M.D., Thomas D. Marcotte, Ph.D., Erin E. Morgan, Ph.D., Matthew Dawson (NPU Manager); Neuroimaging (NI) Core: Gregory G. Brown, Ph.D. (Core Director), Thomas T. Liu, Ph.D., Miriam Scadeng, Ph.D., Christine Fennema-Notestine, Ph.D., Sarah L. Archibald, M.A., John R. Hesselink, M.D., Mary Jane Meloy, Ph.D., Craig E.L. Stark, Ph.D.; Neuroscience and Animal Models (NAM) Core: Cristian L. Achim, M.D., Ph.D. (Core Director), Marcus Kaul, Ph.D., Virawudh Soontornniyomkij, M.D.; Pilot and Developmental (PAD) Core: Mariana Cherner, Ph.D. (Core Director), Stuart A. Lipton, M.D., Ph.D.; Pilot Study Leaders: Jennifer E. Iudicello, Ph.D., Assawin Gongvatana, Ph.D., Rachel D. Schrier, Ph.D., Virawudh Soontornniyomkij, M.D., Marta Massanella, Ph.D.; Administrative Coordinating Core (ACC)–Data Management and Information Systems (DMIS) Unit: Anthony C. Gamst, Ph.D. (Unit Chief), Clint Cushman, B.A. (Unit Manager); ACC–Statistics Unit: Florin Vaida, Ph.D. (Unit Chief), Ian S. Abramson, Ph.D., Reena Deutsch, Ph.D., Anya Umlauf, M.S.; ACC–Participant Unit: J. Hampton Atkinson, M.D. (Unit Chief), Jennifer Marquie-Beck, M.P.H. (Unit Manager); Project 1: Arpi Minassian, Ph.D. (Project Director), William Perry, Ph.D., Mark A. Geyer, Ph.D., Jared W. Young, Ph.D.; Project 2: Amanda B. Grethe, Ph.D. (Project Director), Susan F. Tapert, Ph.D., Assawin Gongvatana, Ph.D.; Project 3: Erin E. Morgan, Ph.D. (Project Director), Igor Grant, M.D.; Project 4: Svetlana Semenova, Ph.D. (Project Director), Athina Markou, Ph.D., James Kesby, Ph.D.; Project 5: Marcus Kaul, Ph.D. (Project Director).

AM has received contract research support from Bristol-Myers Squibb, Forest Laboratories, and Astra-Zeneca and honoraria/consulting fees from AbbVie during the past 3 years. The remaining authors report no financial conflicts of interest. The views expressed in this article are those of the authors and do not reflect the official policy or position of the United States Government.

References

Achat-Mendes C, Ali S, Itzhak Y. Differential effects of amphetamines-induced neurotoxicity on appetitive and aversive Pavlovian conditioning in mice. Neuropsychopharmacology. 2005; 30:1128–1137. [PubMed: 15688084]

Alicata D, Chang L, Cloak C, Abe K, Ernst T. Higher diffusion in striatum and lower fractional anisotropy in white matter of methamphetamine users. Psychiatry Res. 2009; 174:1–8. [PubMed: 19782540]

Bammer, R.; Liu, C.; Po, J.; Moseley, M. Diffusion-weighted magnetic resonance imaging. In: Edelman; Hesselink; Zlatkin; Crues, editors. Clinical Magnetic Resonance Imaging. Elsevier; Philadelphia, PA: 2006. p. 288-319.

Bartzokis G, Beckson M, Lu P, Edwards N, Rapoport R, Wiseman E, Bridge P. Age-related brain volume reductions in amphetamine and cocaine addicts and normal controls: implications for addiction research. Psychiatry Res. 2000; 98:93–102. [PubMed: 10762735]

Bartzokis G, Beckson M, Lu P, Nuechterlein K, Edwards N, Mintz J. Age-related changes in frontal and temporal lobe volumes in men: a magnetic resonance imaging study. Arch Gen Psychiatry. 2001; 58:461–465. [PubMed: 11343525]

Basser, P. Diffusion-tensor MR imaging fundamentals. In: Edelman; Hesselink; Zlatkin; Crues, editors. Clinical Magnetic Resonance Imaging. Elsevier; Philadelphia, PA: 2006. p. 320-332.

Basser P, Mattiello J, LeBihan D. Estimation of the effective self-diffusion tensor from the NMR spin echo. J Magn Reson B. 1994; 103:247–254. [PubMed: 8019776]

Beaulieu C. The basis of anisotropic water diffusion in the nervous system - a technical review. NMR Biomed. 2002; 15:435–455. [PubMed: 12489094]

Berman S, O'Neill J, Fears S, Bartzokis G, London E. Abuse of amphetamines and structural abnormalities in the brain. Ann NY Acad Sci. 2008; 1141:195–220. [PubMed: 18991959]

Bowyer J, Robinson B, Ali S, Schmued L. Neurotoxic-related changes in tyrosine hydroxylase, microglia, myelin, and the blood–brain barrier in the caudate–putamen from acute methamphetamine exposure. Synapse. 2008; 62:193–204. [PubMed: 18081184]

Budde M, Janes L, Gold E, Turtzo L, Frank J. The contribution of gliosis to diffusion tensor anisotropy and tractography following traumatic brain injury: validation in the rat using Fourier analysis of stained tissue sections. Brain. 2011; 134:2248–2260. [PubMed: 21764818]

Büttner A. Review: The neuropathology of drug abuse. Neuropathol Appl Neurobiol. 2011; 37:118–134. [PubMed: 20946118]

Cadet J, Jayanthi S, Deng X. Methamphetamine-induced neuronal apoptosis involves the activation of multiple death pathways. Neurotox Res. 2005; 8:199–206. [PubMed: 16371314]

Chana G, Everall I, Crews L, Langford D, Adame A, Grant I, Cherner M, Lazzaretto D, Heaton R, Ellis R, Masliah E, Group H. Cognitive deficits and degeneration of interneurons in HIV+ methamphetamine users. Neurology. 2006; 67:1486–1489. [PubMed: 17060582]

Chang L, Cloak C, Patterson K, Grob C, Miller E, Ernst T. Enlarged striatum in abstinent methamphetamine abusers: a possible compensatory response. Biol Psychiatry. 2005; 57:967–974. [PubMed: 15860336]

Chanraud S, Zahr N, Sullivan E, Pfefferbaum A. MR diffusion tensor imaging: A window into white matter integrity of the working brain. Neuropsychology Review. 2010; 20:209–225. [PubMed: 20422451]

Chung A, Lyoo I, Kim S, Hwang J, Bae S, Sung Y, Sim M, Song I, Kim J, Chang K, Renshaw P. Decreased frontal white-matter integrity in abstinent methamphetamine abusers. Int J Neuropsychopharmacol. 2007; 10:765–775. [PubMed: 17147837]

Clarke C, Clarke K, Muneyyirci J, Azmitia E, Whitaker-Azmitia P. Prenatal cocaine delays astroglial maturation: immunodensitometry shows increased markers of immaturity (vimentin and GAP-43) and decreased proliferation and production of the growth factor S-100. Developmental Brain Research. 1996; 91:268–173. [PubMed: 8852378]

Cohen, J. Statistical Power Analysis for the Behavioral Sciences. 2. Lawerence Erlbaum Associates; Hillsdale: 1988.

Cox RW. AFNI: software for analysis and visualization of functional magnetic resonance neuroimages. Computers and Biomedical Research. 1996; 29:162–173. [PubMed: 8812068]

Cunha-Oliveira T, Rego A, Oliveira C. Cellular and molecular mechanisms involved in the neurotoxicity of opioid and psychostimulant drugs. Brain Research Reviews. 2008; 58:192–208. [PubMed: 18440072]

Deng X, Ladenheim B, Tsao L, Cadet J. Null mutation of c-fos causes exacerbation of methamphetamine-induced neurotoxicity. J Neurosci. 1999; 19:10107–10115. [PubMed: 10559418]

Dice L. Measures of the amount of ecologic association between species. Ecology. 1945; 26:297–302.

Fantegrossi W, Ciullo J, Wakabayashi K, De La Garza R 2nd, Traynor J, Woods J. A comparison of the physiological, behavioral, neurochemical and microglial effects of methamphetamine and 3,4-methylenedioxymethamphetamine in the mouse. Neuroscience. 2008; 151:533–543. [PubMed: 18082974]

Fumagalli F, Gainetdinov R, Valenzano K, Caron M. Role of dopamine transporter in methamphetamine-induced neurotoxicity: evidence from mice lacking the transporter. J Neurosci. 1998; 18:4861–4869. [PubMed: 9634552]

Henry B, Geyer M, Buell M, Perry W, Young J, Minassian A, Group TMARCT. Behavioral effects of chronic methamphetamine treatment in HIV-1 gp120 transgenic mice. Behavioural Brain Research. 2013; 236:210–220. [PubMed: 22960458]

Jernigan T, Gamst A, Archibald S, Fennema-Notestine C, Mindt M, Marcotte T, Heaton R, Ellis R, Grant I. Effects of methamphetamine dependence and HIV infection on cerebral morphology. Am J Psychiatry. 2005; 162:1461–1472. [PubMed: 16055767]

Johnson G, Badea A, Brandenburg J, Cofer G, Fubara B, Liu S, Nissanov J. Waxholm Space: An image-based reference for coordinating mouse brain research. Neuroimage. 2010; 53:365–372. [PubMed: 20600960]

Kesby J, Heaton R, Young J, Umlauf A, Woods S, Letendre S, Markou A, Grant I, Semenova S. Methamphetamine Exposure Combined with HIV-1 Disease or gp120 Expression: Comparison of Learning and Executive Functions in Humans and Mice. Neuropsychopharmacology. 2015a; 40:1899–1909. [PubMed: 25652249]

Kesby J, Markou A, Semenovan S, Group TMARCT. Cognitive deficits associated with combined HIV gp120 expression and chronic methamphetamine exposure in mice. Eur Neuropsychopharmacol. 2015b; 25:141–150. [PubMed: 25476577]

Kim I, Kim Y, Song H, Lee J, Kwon D, Lee H, Kim M, Yoo D, Chang Y. Reduced corpus callosum white matter microstructural integrity revealed by diffusion tensor eigenvalues in abstinent methamphetamine addicts. Neurotoxicology. 2009; 30:209–213. [PubMed: 19135475]

Kim S, Lyoo I, Hwang J, Chung A, Hoon Sung Y, Kim J, Kwon D, Chang K, Renshaw P. Prefrontal grey-matter changes in short-term and long-term abstinent methamphetamine abusers. Int J Neuropsychopharmacol. 2006; 9:221–228. [PubMed: 15982446]

Kuczenski R, Everall I, Crews L, Adame A, Grant I, Masliah E. Escalating dose-multiple binge methamphetamine exposure results in degeneration of the neocortex and limbic system in the rat. Experimental Neurology. 2007; 207:42–51. [PubMed: 17603040]

Le Bihan D, Johansen-Berg H. Diffusion MRI at 25: exploring brain tissue structure and function. Neuroimage. 2012; 61:324–341. [PubMed: 22120012]

Narayana P, Ahobila-Vajjula P, Ramu J, Herrera J, Steinberg J, Moeller F. Diffusion tensor imaging of cocaine-treated rodents. Psychiatry Research: Neuroimaging. 2009; 171:242–251. [PubMed: 19217266]

Narayana P, Herrera J, Bockhorst K, Esparza-Coss E, Xia Y, Steinberg J, Moeller F. Chronic cocaine administration causes extensive white matter damage in brain: diffusion tensor imaging and immunohistochemistry studies. Psychiatry Research: Neuroimaging. 2014; 221:220–230. [PubMed: 24507117]

Nordahl T, Salo R, Leamon M. Neuropsychological effects of chronic methamphetamine use on neurotransmitters and cognition: a review. J Neuropsychiatry Clin Neurosci. 2003; 15:317–325. [PubMed: 12928507]

Paxinos, G.; Franklin, K. The Mouse Brain in Stereotaxic Coordinates. Academic Press; San Diego: 2001.

Salo R, Fassbender C. Structural, functional and spectroscopic MRI studies of methamphetamine addiction. Curr Topics Behav Neurosci. 2012; 11:321–364.

Salo R, Nordahl T, Buonocore M, Natsuaki Y, Waters C, Moore C, Galloway G, Leamon M. Cognitive control and white matter callosal microstructure in methamphetamine-dependent subjects: a diffusion tensor imaging study. Biol Psychiatry. 2009; 65:122–128. [PubMed: 18814867]

Schwartz D, Mitchell A, Lahna D, Luber H, Huckans M, Mitchell S, Hoffman W. Global and local morphometric differences in recently abstinent methamphetaminedependent individuals. Neuroimage. 2010; 50:1392–1401. [PubMed: 20096794]

Scott J, Woods S, Matt G, Meyer R, Heaton R, Atkinson J, Grant I. Neurocognitive effects of methamphetamine: A critical review and meta-analysis. Neuropsychology Review. 2007; 17:275–297. [PubMed: 17694436]

Segal D, Kuczenski R. An escalating dose binge model of amphetamine psychosis: behavioral and neurochemical characteristics. J Neurosci. 1997; 17:2551–2566. [PubMed: 9065515]

Soontornniyomkij V, Risbrough V, Young J, Soontornniyomkij B, Jeste D, Achim C. Hippocampal calbindin-1 immunoreactivity correlate of recognition memory performance in aged mice. Neuroscience letters. 2012; 10:161–165. [PubMed: 22503902]

Soontornniyomkij V, Risbrough V, Young J, Wallace C, Soontornniyomkij B, Jeste D, Achim C. Short-term recognition memory impairment is associated with decreased expression of FK506 binding protein 51 in the aged mouse brain. Age. 2010; 32:309–322. [PubMed: 20422297]

Thomas D, Kuhn D. Attenuated microglial activation mediates tolerance to the neurotoxic effects of methamphetamine. J Neurochem. 2005; 92:790–797. [PubMed: 15686480]

Thompson P, Hayashi K, Simon S, Geaga J, Hong M, Sui Y, Lee J, Toga A, Ling W, London E. Structural abnormalities in the brains of human subjects who use methamphetamine. J Neurosci. 2004; 24:6028–6036. [PubMed: 15229250]

Tobias M, O'Neill J, Hudkins M, Bartzokis G, Dean A, London E. White-matter abnormalities in brain during early abstinence from methamphetamine abuse. Psychopharmacology (Berl). 2010; 209:13–24. [PubMed: 20101394]

Zhu J, Xu W, Angulo J. Disparity in the temporal appearance of methamphetamine-induced apoptosis and depletion of dopamine terminal markers in the striatum of mice. Brain Res. 2005; 1049:171–181. [PubMed: 16043139]

Highlights

- We examined brain microstructure with *in vivo* diffusion tensor imaging of mice
- A methamphetamine binge regimen produced long lasting microstructural brain changes
- Four different patterns of signal change were observed in white and gray matter
- Findings highlight distributed and differential methamphetamine effects
- Methamphetamine likely changes brain tissue differentially depending on tissue type

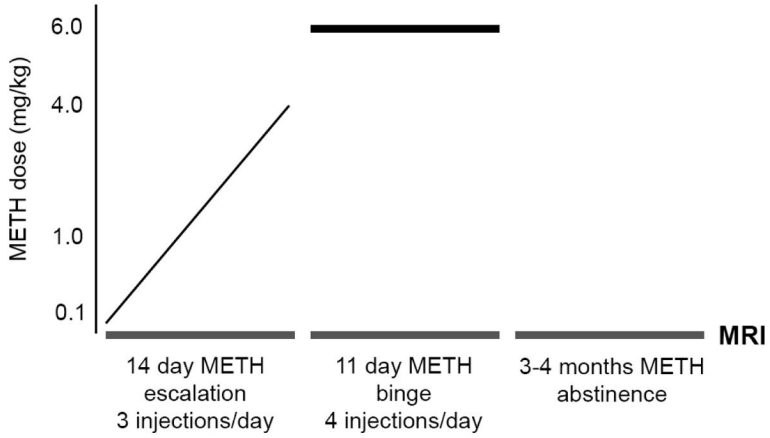

Figure 1.
Experimental Design. METH: Methamphetamine; MRI: Magnetic Resonance Imaging.

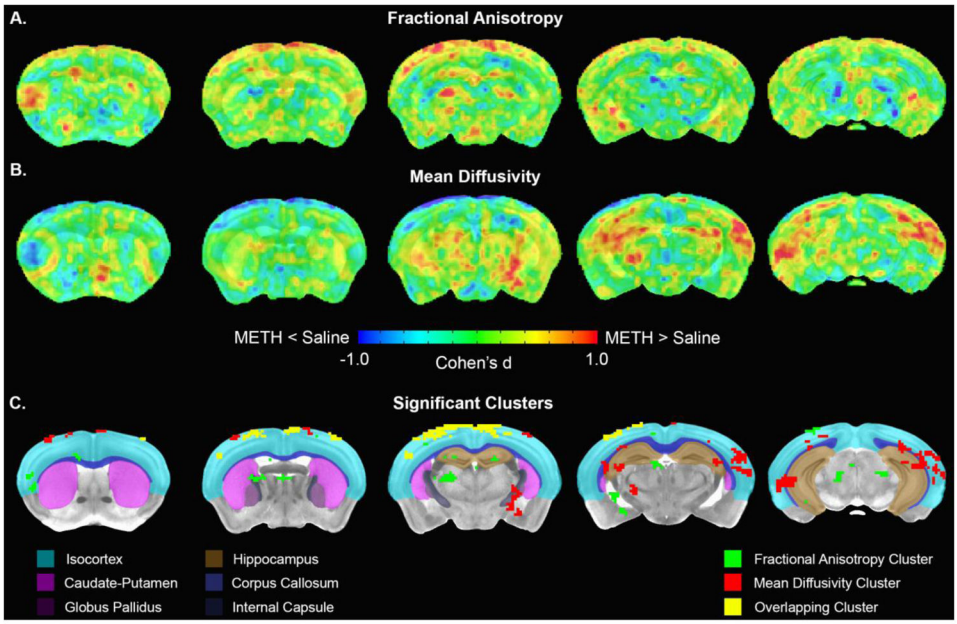

Figure 2.

Comparison of methamphetamine (METH) exposed mice to saline control mice. All images are coronal slices in neurological view (left side of brain is the left hemisphere). A) Fractional anisotropy (FA) parametric maps and B) Mean diffusivity (MD) parametric maps demonstrating Cohen's d effect sizes. Maps were resampled to 100μm isotropic and smoothed full width half mass by 150μm for presentation. Positive values reflect higher FA/MD in the METH sample compared to saline sample and negative values represent lower FA/MD in the METH sample. C) Clusters where differences were significant at a corrected p-value of 0.05.

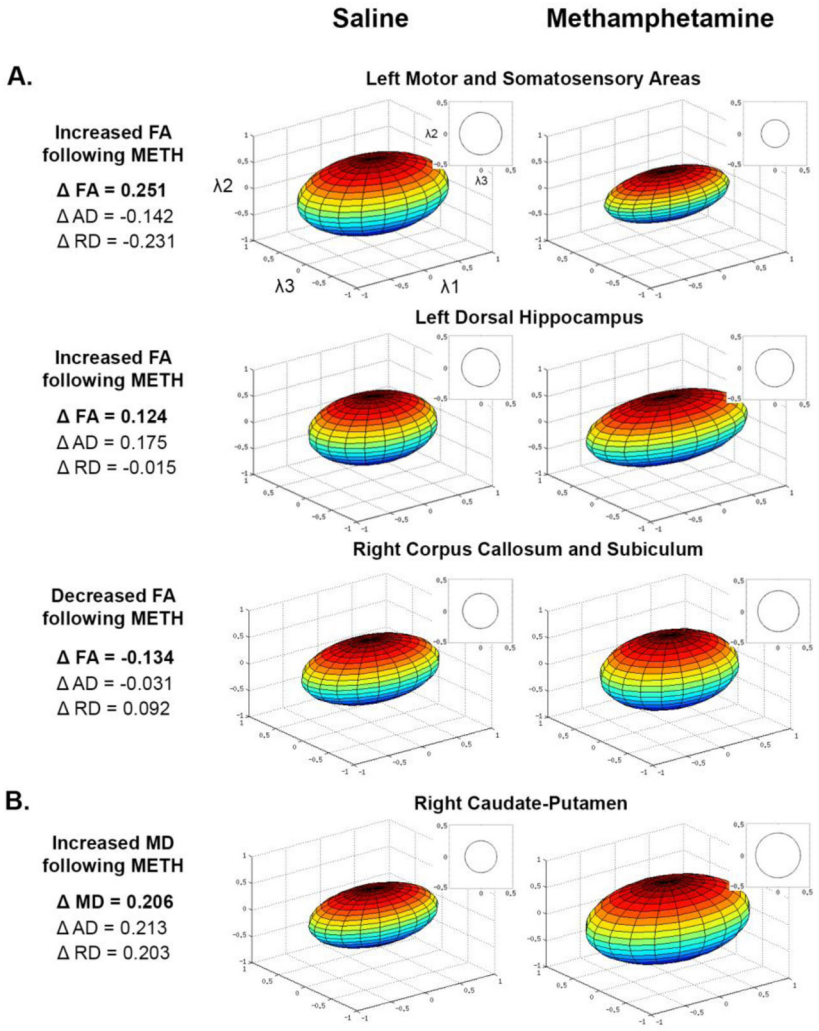

Figure 3.

Examples of group averaged diffusivity and fractional anisotropy values demonstrating the geometric shape of ellipsoids. Average axial diffusivity values were used for the λ1 axis and radial diffusivity values were used for λ2 and λ3 axes as radial diffusivity is the average of λ2 and λ3 represented by the circle next to ellipsoid. A) Two example regions demonstrating increased fractional anisotropy in methamphetamine-exposed mice compared to saline control mice and one example region demonstrating decreased fractional anisotropy B) One example region demonstrating increased mean diffusivity in methamphetamine-exposed mice. METH: methamphetamine; FA: fractional anisotropy; MD: mean diffusivity; AD: axial diffusivity; RD: radial diffusivity.

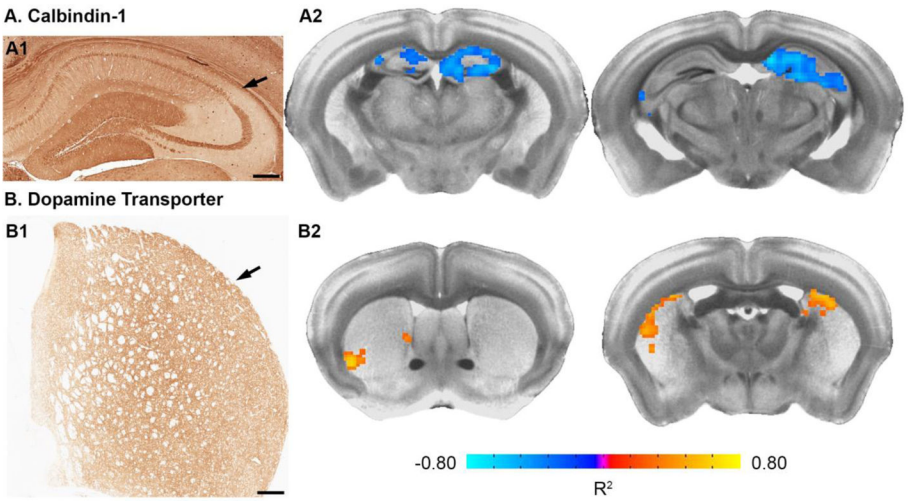

Figure 4.

Representative immunoreactivity patterns for A1) calbindin-1 in the dorsal hippocampal formation and B1) dopamine transporter in the caudate-putamen from the same mouse brain. Arrows indicate the lateral borders of hippocampal CA1 (A1) and caudate-putamen (B1) in coronal plane. Scale bars = 300μm. Associations between A2) mean diffusivity and calbindin-1 in dorsal hippocampus; and B2) mean diffusivity and dopamine transporter in caudate-putamen. R^2 values have the sign of the correlation preserved to illustrate directionality and were thresholded at $R^2 \pm 0.25$. The same cluster threshold used in the main analyses of 0.081μL was then applied. Images are coronal slices in neurological view (left side of brain is the left hemisphere). Maps were resampled to 100μm isotropic and smoothed full width half mass by 150μm for presentation. Positive values represent a positive relationship between mean diffusivity and immunoreactivity intensities, and negative values a negative relationship.

Table 1

Regions of significant fractional anisotropy differences between methamphetamine exposed and saline control mice

Region		Fractional Anisotropy				Radial Diffusivity				Axial Diffusivity			
	Volume	SALINE	METH	Meth-Saline	hedge's g	SALINE	METH	Meth-Saline	hedge's g	SALINE	METH	Meth-Saline	hedge's g
METH > SALINE													
Isocortex													
L Motor/Somatosensory Areas	2.10 μL	0.284 ± 0.09	0.499 ± 0.21	0.215	1.273	0.668 ± 0.19	0.437 ± 0.21	−0.231	−1.116	1.002 ± 0.27	0.860 ± 0.22	−0.142	−0.561
R Motor/Somatosensory Areas	0.891 μL	0.258 ± 0.07	0.438 ± 0.20	0.180	1.147	0.701 ± 0.12	0.518 ± 0.20	−0.183	−1.066	1.022 ± 0.19	0.929 ± 0.20	−0.093	−0.462
L Somatosensory Area	0.176 μL	0.218 ± 0.06	0.451 ± 0.33	0.234	0.935	0.811 ± 0.35	0.497 ± 0.36	−0.314	−0.857	1.119 ± 0.46	0.883 ± 0.38	−0.236	−0.544
L Motor Area/Medial Temporal Lobes	0.243 μL	0.270 ± 0.08	0.504 ± 0.29	0.234	1.049	0.634 ± 0.12	0.421 ± 0.29	−0.213	−0.918	0.939 ± 0.16	0.803 ± 0.25	−0.136	−0.623
L Dorsal Hippocampus	0.176 μL	0.227 ± 0.06	0.351 ± 0.11	0.124	1.343	0.602 ± 0.05	0.587 ± 0.10	−0.015	−0.182	0.840 ± 0.07	1.015 ± 0.22	0.175	1.023
R Dorsal Hippocampus	0.176 μL	0.260 ± 0.07	0.372 ± 0.10	0.112	1.250	0.627 ± 0.08	0.545 ± 0.05	−0.082	−1.203	0.917 ± 0.14	0.977 ± 0.16	0.060	0.386
L Ventral Hippocampus	0.149 μL	0.240 ± 0.05	0.349 ± 0.09	0.109	1.437	0.627 ± 0.07	0.602 ± 0.12	−0.025	−0.244	0.896 ± 0.12	1.003 ± 0.19	0.107	0.647
L Amygdala	0.081 μL	0.274 ± 0.13	0.458 ± 0.15	0.184	1.268	0.664 ± 0.24	0.557 ± 0.17	−0.107	−0.502	0.990 ± 0.28	1.141 ± 0.30	0.151	0.504
Brain Stem													
L Thalamus (lateral aspect)	0.419 μL	0.309 ± 0.04	0.342 ± 0.06	0.033	0.623	0.587 ± 0.07	0.670 ± 0.20	0.083	0.529	0.941 ± 0.11	1.101 ± 0.23	0.160	0.850
White Matter Involvment													
L Corpus Callosum (genu)/Motor Area	0.081 μL	0.234 ± 0.06	0.322 ± 0.06	0.088	1.422	0.712 ± 0.23	0.624 ± 0.14	−0.088	−0.452	0.994 ± 0.27	1.009 ± 0.20	0.015	0.062
METH < SALINE													
Brain Stem													
L Thalamus (medial aspect)	0.203 μL	0.345 ± 0.08	0.261 ± 0.07	−0.084	−1.087	0.577 ± 0.10	0.650 ± 0.08	0.073	0.785	0.961 ± 0.15	0.953 ± 0.15	−0.009	−0.052
L Midbrain Grey Matter	0.135 μL	0.404 ± 0.09	0.274 ± 0.06	−0.130	−1.661	0.516 ± 0.05	0.582 ± 0.06	0.066	1.155	0.982 ± 0.18	0.869 ± 0.15	−0.113	−0.664
R Midbrain Grey Matter	0.108 μL	0.389 ± 0.08	0.284 ± 0.07	−0.105	−1.358	0.518 ± 0.04	0.577 ± 0.09	0.059	0.811	0.956 ± 0.2	0.872 ± 0.13	−0.084	−0.487
White Matter Involvment													
L Internal Capsule/caudate-putamen	0.095 μL	0.382 ± 0.09	0.253 ± 0.07	−0.129	−1.559	0.591 ± 0.14	0.828 ± 0.46	0.237	0.665	1.076 ± 0.22	1.169 ± 0.51	0.093	0.227
R Corpus Callosum (posterior forceps)/Subiculum	0.095 μL	0.346 ± 0.15	0.212 ± 0.06	−0.134	−1.154	0.553 ± 0.15	0.645 ± 0.14	0.092	0.616	0.914 ± 0.22	0.883 ± 0.22	−0.031	−0.137

L: left; R: right; METH: methamphetamine exposed mice; SALINE: saline control mice. Radial and Axial diffusivity values are $x10^{-3}$ mm^2/second. Data are expressed as mean ± standard deviation.

Table 2

Regions of significant mean diffusivity differences between methamphetamine exposed and saline control mice

Region		Mean Diffusivity				Radial Diffusivity				Axial Diffusivity			
	Volume	SALINE	METH	Meth-Saline	hedge's g	SALINE	METH	Meth-Saline	hedge's g	SALINE	METH	Meth-Saline	hedge's g
METH > SALINE													
Isocortex and Medial Temporal Lobes													
L Visual Area	0.635 μL	0.620 ± 0.07	0.839 ± 0.16	0.219	1.697	0.506 ± 0.08	0.704 ± 0.15	0.198	1.580	0.847 ± 0.07	1.110 ± 0.20	0.263	1.676
R Auditory Area/Hippocampus	1.553 μL	0.607 ± 0.13	0.814 ± 0.17	0.207	1.320	0.509 ± 0.15	0.704 ± 0.15	0.195	1.261	0.803 ± 0.15	1.035 ± 0.22	0.232	1.186
L Perirhinal and Ectorhinal Areas/Hippocampus	0.459 μL	0.596 ± 0.11	0.828 ± 0.25	0.232	1.149	0.499 ± 0.13	0.693 ± 0.22	0.194	1.031	0.789 ± 0.09	1.097 ± 0.33	0.308	1.214
L Dorsal Hippocampus/Corpus Callosum	0.243 μL	0.641 ± 0.08	0.804 ± 0.22	0.163	0.941	0.545 ± 0.09	0.680 ± 0.21	0.135	0.799	0.833 ± 0.11	1.052 ± 0.28	0.219	0.984
R Dorsal Hippocampus	0.216 μL	0.650 ± 0.04	0.722 ± 0.06	0.072	1.359	0.546 ± 0.05	0.603 ± 0.04	0.057	1.226	0.857 ± 0.11	0.959 ± 0.13	0.102	0.819
R Amygdala	0.081 μL	0.689 ± 0.11	0.903 ± 0.24	0.214	1.097	0.544 ± 0.11	0.701 ± 0.25	0.157	0.778	0.978 ± 0.19	1.307 ± 0.27	0.329	1.357
Basal Ganglia													
R Caudoputamen	0.095 μL	0.622 ± 0.11	0.828 ± 0.24	0.206	1.056	0.503 ± 0.12	0.706 ± 0.21	0.203	1.139	0.859 ± 0.14	1.072 ± 0.30	0.213	0.871
Brain Stem													
L Hypothalamus	0.122 μL	0.641 ± 0.06	0.722 ± 0.05	0.081	1.427	0.511 ± 0.09	0.574 ± 0.08	0.063	0.719	0.902 ± 0.12	1.018 ± 0.15	0.116	0.825
White Matter Involvment													
L Cerebral Peduncle/Amygdala	0.095 μL	0.669 ± 0.07	0.787 ± 0.11	0.118	1.231	0.524 ± 0.09	0.627 ± 0.11	0.103	0.990	0.960 ± 0.15	1.107 ± 0.15	0.147	0.950
R Internal Capsule/Amygdala	0.297 μL	0.638 ± 0.05	0.797 ± 0.17	0.159	1.210	0.484 ± 0.10	0.631 ± 0.18	0.147	0.969	0.945 ± 0.14	1.130 ± 0.19	0.185	1.069
R Corpus Callosum (genu)/ Anterior Cingulate	0.162 μL	0.647 ± 0.07	0.737 ± 0.07	0.090	1.247	0.544 ± 0.09	0.628 ± 0.05	0.084	1.131	0.852 ± 0.09	0.954 ± 0.11	0.102	0.980
METH < SALINE													
Isocortex													
L Motor/Somatosensory Areas	2.930 μL	0.834 ± 0.24	0.571 ± 0.20	−0.263	−1.159	0.723 ± 0.21	0.456 ± 0.23	−0.267	−1.174	1.056 ± 0.31	0.802 ± 0.18	−0.254	−0.981
R Motor/Somatosensory Areas	1.040 μL	0.802 ± 0.13	0.570 ± 0.16	−0.232	−1.537	0.682 ± 0.10	0.440 ± 0.18	−0.242	−1.595	1.042 ± 0.20	0.831 ± 0.15	−0.211	−1.164

L: left; R: right; METH: methamphetamine exposed mice; SALINE: saline control mice. All diffusivity values (Mean, Radial, and Axial) are $x10^{-3}$ mm^2/second. Data are expressed as mean ± standard deviation.